A Study on the Classification of Geological Background Source Cadmium Migration Phases in Zhejiang Provence, China

Wenda Zhou
Zhejiang Institute of Geosciences
Xinze Lu
Zhejiang Institute of Geosciences
Chunlei Huang
Zhejiang Institute of Geosciences
Jinghe Wang
Zhejiang Juhua Chemical and Mining Industry Co., Ltd
Kegan Guo
Yangtze River Ecological Protection Group Company of Limited Liability
Shuyun Xie (tinaxie@cug.edu.cn)
State Key Laboratory of Geological Processes and Mineral Resources (GPMR), School of Earth Sciences, China University of Geosciences

Research Article

Keywords: Cadmium, Migration, Stage, Weather Degree, Iron-Sediment

Posted Date: June 8th, 2023

DOI: https://doi.org/10.21203/rs.3.rs-3007568/v1

Abstract

The release of cadmium during the natural weathering process of cadmium-containing strata constitutes a significant source of cadmium pollution in both water and soil. The Hetang Formation, located in western Zhejiang Province in China, is a typical example of a cadmium-rich black shale stratum. The bottom coal seam of this formation has been found to contain high levels of cadmium, with concentrations reaching up to 11.2 mg/kg. The continuous weathering and erosion of cadmium-bearing bedrock by fluvial processes results in the release of cadmium, leading to geological background cadmium contamination of downstream soils. This study relies on the strong adsorption characteristics of iron-sediment for cadmium during migration and uses FE-SEM, EDS, optical microscopes and other means to observe the distribution of iron elements in rock fragments of different weathering degrees in the Hetang Formation in river channels. The aim is to explore the state of cadmium from geological background sources during migration. By comparing detritus from upstream and downstream sections of the river channel, it was determined that under weathering conditions, the occurrence state of geological background source cadmium could be divided into three distinct stages: unweathered stage; intra-detritus migration stage; and completely weathered stage. Furthermore, after leaving the Hetang Formation shale outcrop area, there was a sharp decrease in content for Hetang Formation detritus. At this point geological background source cadmium had largely escaped from constraints imposed by rock structure and had come into full contact with water. The findings from this research deepen our understanding regarding migration patterns for geological background source cadmium. They also reveal formation processes for geological background source cadmium pollution and provide a theoretical basis for identification and treatment for geological background source cadmium pollution.

1 Introduction

The issue of soil heavy metal pollution has garnered significant attention due to its increasing severity in the wake of industrial and mining development (Burbacher et al., 2015; Kasuya,2000). Approximately 14.3% of soil survey sites across Europe have been identified as requiring remediation for heavy metal contamination (Mahar et al., 2016). Cadmium, in particular, poses a considerable threat as a primary pollutant due to its easy accumulation, high mobility, and high toxicity (Gobe and Crane, 2010; Jarup et al., 1998). In China, the majority of soil affected by heavy metal pollution is contaminated with cadmium (China soil pollution investigation bulletin, 2014).

Cadmium contamination can be classified into two categories based on the influence of human activities: geological backgrounds pollution and anthropogenic pollution. The former is intimately linked to the natural weathering of strata with high cadmium concentrations (Mndrescu et al.,2022; Islam et al.,2018). Cadmium within these strata accumulate in metal sulfides such as pyrite and sphalerite in an isostructural manner (Liu et al.,2017; Cullen and Maldonado,2013). As weathering continues, rocks containing cadmium disintegrate and fragment, exposing their metal sulfides to air and water where they undergo oxidation. Ultimately, metallic elements such as cadmium and iron are released into water in their ionic forms (Yang et al.,2018). In contrast to anthropogenic pollution sources, cadmium contamination from geological backgrounds is characterized by a slower rate of release and a longer duration.

Globally, black shale is generally rich in Cd (Liu et al.,2017;Liu et al.,2020; Lavergren et al., 2009). The Low Cambrian Hetang Formation in the eastern China represents a quintessential region with high geological background levels of cadmium (Xin and Sui,2022 Zhao et al.,2018). Concurrently, abundant stone coal resources are present at the base of the Hetang Formation (Song,2009). Historically, haphazard extraction of stone coal resulted in a substantial expansion of Hetang Formation strata exposed to water and air. This exposure produced copious amounts of acid mine drainage (AMD) enriched with iron and cadmium that persistently contaminated proximate water systems and soil. Consequently, to devise a scientifically sound strategy for managing cadmium pollution, it is imperative to elucidate the migration patterns of cadmium originating from geological background sources.

Currently, the assessment of mixed cadmium pollution from both geological background and anthropogenic sources primarily employs the geo-accumulation index (Williams and Antoine,2020; Liu et al.,2021) and multi-element geochemical valuation methods (Han et al.,2022; Hamon et al.,2004). However, the methodology for determining the constant K value within Muller's cumulative index formula, which accounts for fluctuations in background values induced by diagenesis, and its associated conditions of use are absent. Consequently, it is no longer capable of fulfilling the requirements for a scientific evaluation of heavy metal contamination across regions with varying geological backgrounds. Conversely, due to the shared origin of anthropogenic and geological background pollution, it is challenging to discern their respective contributions using geochemical analysis techniques such as cadmium isotopes. As such, there is an exigent need for meticulous investigation into the processes underlying cadmium pollution from high cadmium level geological backgrounds regions. Such research would elucidate the migration patterns of cadmium and furnish a foundation for scientifically evaluating the proportion of cadmium pollution attributable to geological background sources within areas affected by complex pollution.

The geological background source of cadmium pollution can be attributed to two distinct processes: the leaching of cadmium-rich parent rocks on slopes exposed to the surface environment, and the erosion of cadmium-rich strata by hydrodynamic force (Chen et al., 2014).

The weathering of parent rocks can be further classified into chemical and physical weathering (Riebe et al.,2003; Qin et al.,2006). Notably, due to direct exposure to water erosion, the rate of erosion for riverbed bedrock is comparatively rapid (Tarun et al.,2012). This is particularly evident in

hilly terrain where there is a significant elevation difference between the upstream and downstream sections of a river and where water flow is relatively swift. Under these conditions, chemical weathering and hydraulic action result in a more rapid rate of weathering for cadmium-rich parent rocks in riverbeds compared to those on slopes (Inoue et al., 2017; Dosseto et al., 2014). Consequently, this represents the most significant geological source for cadmium pollution at present.

The process of weathering involves numerous factors that contribute to cadmium pollution caused by geological background. These factors include rock collapse, mineral dissolution and element migration within water systems. The release and migration of cadmium is influenced by various environmental conditions such as temperature, pH levels and ion strength (Yang et al., 2021; Lasaga et al.,1994). Compared to cadmium pollution caused by anthropogenic activities, the process caused by geological background is considerably more complex. However, these differences also provide an opportunity to distinguish between geological background causes and anthropogenic cadmium pollution from the same source. This study focuses on the Hetang formation in Kaihua County, Zhejiang Province. Given that approximately 90% of cadmium is adsorbed by iron-sediment during migration (Zhou et al.,2020), this research utilizes the migration characteristics of iron elements to reconstruct the migration and enrichment patterns of geological background source cadmium resulting from natural weathering of Hetang formation.

2 Geological Conditions and Samples

2.1 Geological Background of the Study Area

The study area encompasses Cuntou Town and Huabu Town in Kaihua County, located in the western region of Zhejiang Province. The Majin River traverses this area, where Sinian-Ordovician strata are exposed (Fig. 1). The topography of the study area is characterized by hills and the river exhibits downcutting behavior. Bedrock is visible and an abundance of pebbles with diameters ranging from 1–20 cm have accumulated within the river channel. The proportion of bottom mud composed of fine-grained silt with particle sizes less than 0.5 cm is below 5%. Between May and September each year, precipitation accounts for approximately 65% of the region's annual rainfall total and often results in a substantial increase in Majin River's discharge due to afternoon thunderstorms. Over an extended period measured in years, fine-grained sediments within the river are subject to migration.

2.2 Sample Collection

To ascertain the origin of cadmium within the geological background of the study area, eight varieties of exposed bedrock outcrop samples were obtained. During collection, the weathered layer on the surface was removed to a depth of 5cm.

To ascertain the spatial distribution of cadmium derived from geological background sources, this investigation established three sample locations within the Hetang formation distribution area and two sample locations downstream of the Hetang formation strata distribution area (Fig. 1). Five riverbed sediment samples were procured at intervals of approximately 10 kilometers. Sample 1 was situated in the Hetang formation exposure zone and approximately 20 meters downstream from the effluent discharge point for AMD emanating from an abandoned stone coal mine. All sediment samples were obtained using stainless steel spades at concave banks during the winter low-water season, with pebbles exceeding 2 centimeters in diameter being removed.

3 Methods

3.1 Extraction of rock fragments from sediment

In the research area, sediment comprises rock debris and mineral particles ranging in size from millimeters to micrometers. To mitigate interference from fine particles and organic matter, sediment samples were subjected to washing and subsequently segregated into rock debris and minerals based on particle size. Utilizing the United States Department of Agriculture's (USDA) soil particle size classification scheme (Wang et al.,2014), nylon screens with mesh sizes of 18, 32, and 150 were employed to categorize sediment particle sizes into silt and clay (< 150 mesh), fine sand (32–150 mesh), medium sand (18–32 mesh), and coarse sand (> 18 mesh). During the sieving process, samples were rigorously agitated to disintegrate agglomerate structures between fine particles.

Sediment samples of 18–32 mesh, 32–150 mesh, and < 150 mesh were subjected to a series of treatments. Firstly, the samples were rinsed with clean water and subjected to 60HZ ultrasonic oscillation for 30 seconds until no obvious suspended solids remained. This step removed small minerals adhering to the surface of particles. Secondly, the samples were soaked in a solution of 30% hydrogen peroxide at 60°C for 30 minutes and then subjected to ultrasonic oscillation at 60Hz for 30 seconds before being rinsed with clean water. This process was repeated until the hydrogen peroxide solution was clear (Note: there is a certain probability that foam will overflow quickly during the hydrogen peroxide soaking process!). This step removed most organic matter and small particles adhered by organic matter (Miller et al.,2009). Thirdly, the samples were soaked in a shaking condition with a solution of 15% HCl for 30 minutes and then subjected to ultrasonic oscillation at 60Hz for 30s before being rinsed with clean water. This process was repeated until the solution was almost colorless. By lowering the pH value to increase the solubility of

iron elements, this step removed iron precipitates from anthropogenic pollution sources adhering to the surface of rock debris (Zhu et al.,2021). After undergoing these steps, clean rock debris and quartz particles of various particle sizes that can be observed by instruments were obtained.

3.2 Observation of rock debris morphology at different scales

3.2.1 Identification of debris type and morphological observation

Rock debris and minerals were examined utilizing a DM2000 optical microscope. An external direct light source was employed in conjunction with 5x, 10x and 20x apertures (Kleven et al.,2009;Rola et al.,2013).

Utilizing microscopic analysis of rock fragment color, morphology and iron-sediment adhesion status in conjunction with previously acquired data on stratum exposure within the study area and empirical observations of stratum outcrops, statistical methods were employed to select rock debris from the Hetang formation for detailed examination of their microstructure.

3.2.2 Microscopic observation of mineralogical patterns on the surface of rock debris

Utilizing an optical microscope, rock debris and quartz specimens are selected for observation via a scanning electron microscope. Subsequently, the specimens are affixed using epoxy resin and the cross-sections are ground to a flat surface. Carbon coating is then applied in preparation for further analysis.

All separated samples have been investigated by using Field Emission Scanning Electron Microscope (FE-SEM) imaging and EMS analyses. FE-SEM imaging were made on a Apreo S instrument, with working distances of 7 mm to 17mm and acceleration voltages of 5 kV to15 kV(Liu et al., 2017; Tan et al., 2015).

EDS was carried out using ESCA+ (Oxford Instruments,Germany) and the resolution ratio was 0.4%. The beam size of the electron beam gun was ~ 75 nm in diameter. The energy resolution was 0.5 eV. The proportions of oxygen were obtained by stoichiometry (Rusk and Reed, 2002).

3.3 The analysis of rock elemental composition

Following pretreatment procedures, bedrock and sediment samples obtained from the study area were analyzed for cadmium and iron content utilizing a NexION 2000 ICP-MS instrument manufactured by PerkinElmer (Ma et al.,2018). During analysis, the RF transmission power was set to 1200 W and a glass concentric nebulizer was employed. Each sample underwent triplicate analysis. Standard substances GSS-1, GSS-11, and GSS-16 from the Institute of Geophysical and Geochemical Exploration at the Chinese Academy of Geological Sciences were utilized for sample analysis.

4 Results and discussion

4.1 Geological background source of cadmium element

Upon examination of the strata traversed by Majin river within the research area, it was determined that the primary stratum containing cadmium is the cambrian Hetang formation. The cadmium content within this stratum exceeds that of other strata by two orders of magnitude and surpasses the abundance value of cadmium in China's continental lithosphere. This stratum is characteristic for its enrichment in cadmium (Li and Ni,1997) (Table 1). Cadmium elements are predominantly concentrated in metal sulfides such as pyrite through a process of isomorphism (Bostick et al.,2000; Song,2009). The Hetang formation comprises gray-black carbonaceous mudstone and powdery sandstone mudstone. The pyrite content at the base of this formation's coal seam reaches 35.1% (Fig. 2).

Table 1
Cadmium content of strata in the study area(mg/kg)

Formation	Yinzhuwu (O_1y)	Xiyangshan ($Є_3x$)	Huayansi ($Є_3h$)	Yangliugang ($Є_2y$)	Dachenling ($Є_1d$)	Hetang ($Є_1h$)	Banqiaoshan (Z_2b)	Doushantuo (Z_2d)	The prevalence of cadmium within the lithospheric composition of China
Cadmium Content	0.180	0.044	0.042	0.360	0.033	11.260	0.069	1.410	0.061

4.2 The occurrence state of cadmium from geological background sources

The occurrence state of geological background sources cadmium is intimately associated with the weathering degree by the Hetang formation. In a Hetang formation debris from sample 1, a partial disintegration of rock microstructure is observed within area B where pyrite enriched in cadmium has undergone weathering, resulting in an abundance of dissolution cavities. Some of these cavities have even been filled with granular iron-sediment. In contrast, area A exhibits no significant damage to rock structure or mineral morphology and inter-mineral contacts remain tight (Fig. 3). Iron released through pyrite dissolution migrates and precipitates via interconnected pore spaces within the rock debris (Fig. 4).

As the weathering process progresses, cadmium begin to diffuse within rock debris. Pyrite within the Hetang formation rock debris undergoes complete dissolution, leaving behind numerous mold cavities. Cadmium elements uniformly infiltrate rock debris interconnected pores with iron-sediment (Fig. 5). With increasing weathering duration, iron elements are gradually released outward via interconnected pores and adhere to rock debris surfaces in a lacquer-like manner (Fig. 6A). Based on the morphology of iron-sediment and their yellow-brown characteristics (Fig. 6B), it can be inferred that at this point in time, iron-sediment containing cadmium elements formed through geological background diagenesis have undergone a transformation from unstable ferrihydrite to stable siliceous limonite (Fig. 6C). Energy spectrum analysis indicates that cadmium-containing iron-sediment remain primarily concentrated within rock debris and no significant enrichment of iron elements is observed on rock debris surfaces. Furthermore, the adhesion strength between geological background diagenetic iron-sediment and rock debris is exceedingly high; even after repeated treatment with HCl solution, H_2O_2 solution and 60Hz ultrasound, large-scale peeling of lacquer-like iron-sediment on rock debris surfaces is not observed (Fig. 6A). This phenomenon suggests that the migration process of cadmium from geological background sources is intimately linked to the weathering process of rock debris; prior to complete weathering of rock debris, cadmium migration adheres to a rock migration pattern

The stability of rock debris structure plays a crucial role in regulating the migration of geological background sources cadmium. Upon complete dissolution of pyrite, numerous pores ranging from 40–100μm in diameter emerge within the Hetang formation rock debris. This results in a loosening of the rock debris structure and facilitates pore water infiltration between particles. Consequently, relatively loose clay minerals within deposits undergo softening and ultimately lead to a substantial reduction in the mechanical stability of rock debris (Feng et al.,2009). During the migration process of rock debris, external forces such as hydrodynamics cause preferential fracturing in weak areas between injection mold pores, leading to further fragmentation of rock debris (Fig. 7). This process exposes large quantities of cadmium-containing iron-sediment distributed within the rock debris to the water environment. Sudden alterations in environmental factors including pH and Eh induce migration of cadmium initially adhered to iron-sediment on inner walls of interconnected pores towards external surroundings. As weathering progresses and fragmentation intensifies, all cadmium-containing iron-sediment within pores eventually enter the water environment.

In summary, the migration process of geological background source cadmium can be divided into three stages according to the spatial relationship between cadmium and rock debris. In the first stage, cadmium exist in pyrite within the Hetang formation rock debris (Fig. 8A); In the second stage, pyrite undergoes dissolution, most of the cadmium-containing iron-sediment fill the pores within the rock debris, and a small amount migrates to the surface of the rock debris through pores and adheres tightly (Fig. 8B); In the third stage, rock debris gradually disintegrates until fine single minerals are exposed to water environment (Fig. 8C).

4.3 The occurrence state of cadmium in different geological background areas of the river channel

The hydrodynamic conditions in the upper and lower segments of the river influence the particle size distribution of the rock debris (Landeghem et al.,2012), which in turn depends on the weathering degree of the rock debris (Liang et al.,2013; Chen et al.,2006). Hence, the occurrence state of geological background sources cadmium varies across different regions due to different weathering levels during the migration process.

The research area exhibits consistent river channel width and drop, with stable hydrodynamic conditions in both upstream and downstream regions. Analysis of the hydrodynamic model and the weighing results of samples with varying particle sizes indicates that the particle size composition of rock debris in the upstream and downstream regions is consistent under hydrodynamic sorting (Hawleyn, 2000; Philipp et al.,2009)(Fig. 9). However, a significant decrease in the content of Hetang formation rock debris is observed with increasing migration distance, with a sharp drop in content when sample 4 exits the Hetang formation distribution area (Fig. 10). This sharp change in Hetang formation rock debris content presents a contradiction with the stability of rock debris particle size composition in upstream and downstream regions. The observed phenomenon suggests that, in comparison to sandstone, siltstone, and quartz, the weathering resistance of Hetang formation rock debris, as mudstone-siltstone rock, is notably weaker (Boardman, 2015). The research area, located in a subtropical monsoon climate with hilly terrain, experiences concentrated migration of river bottom mud during afternoon thunderstorms in the spring and summer seasons (Zhang et al.,2020). As a result, Hetang formation rock debris experiences a prolonged weathering period prior to migration, allowing sufficient time for pore water to promote the dissolution of pyrite and the transition of cadmium in the rock debris to a relatively unstable second stage within the rock debris structure. The impact of hydrodynamics during migration causes the Hetang formation rock debris in the second occurrence state stage to fragment and transition to the third stage.

An analysis of the distance of various samples from the Hetang Formation distribution area, in conjunction with the observed changes in the content of Hetang Formation rock debris of different particle sizes, indicates that the geological background source cadmium in the Hetang

Formation distribution area is in the first and second occurrence state stages. As the distance from the Hetang Formation stratum exceeds 10km, the cadmium-containing rock debris transition into the third occurrence state stage. At this stage, the geological background source cadmium is no longer under the control of rock debris. Instead, fine cadmium-containing iron-sediment are either adsorbed by other substances in the bottom mud or undergo rapid long-distance migration with the water flow.

5 Conclusion

The current geological context of cadmium pollution primarily originates from the ongoing release of cadmium elements during the natural weathering of cadmium-containing rocks. Through an analysis of the micro-morphology of cadmium-containing pyrite and its weathering products within rock debris of the Hetang Formation located in the river channel at varying stages of weathering in the study area, this article categorizes the migration process of cadmium-bearing rock fragments into three distinct phases: (1) The presence of cadmium within the pyrite of Hetang Formation rock debris; (2) The dissolution of pyrite, resulting in the majority of cadmium being uniformly distributed within the pores of rock fragments alongside iron-sediment; (3) The disintegration of rock debris, leading to the exposure of cadmium-containing iron precipitates originally located within the pores to the aquatic environment.

This study examines the influence of the weathering rate of rock debris from the Hetang Formation on the distribution of cadmium. The analysis is based on the composition of rock debris grain sizes in different regions of the river, as well as the content of rock debris from the Hetang Formation. Preliminary findings suggest that during the time interval between two instances when the river flow rate exceeds the migration rate of rock debris from the Hetang Formation, the majority of this material undergoes weathering, resulting in the formation of finer particles that are transported further downstream. This leads to a marked decrease in the content of clastic material from the Hetang Formation after it has moved beyond the distribution range of the parent rock.

This study presents preliminary findings on the categorization of the geological background source cadmium migration phases. Further research within watersheds could refine and enhance our understanding of the patterns of geological background sources cadmium migration.

References

1. Boardman J (2015) Rapid and selective clast weathering on an alluvial fan, eastern karoo, south africa. Catena 126: 37–42. https://doi.org/10.1016/j.catena.2014.10.036
2. Bostick BC, Fendorf S, Bowie BT, Griffiths PR (2000) Influence of cadmium sorption on FeS2 oxidation. Environmental Science & Technology 34(8):1494–1499. https://doi.org/10.1021/es990742w
3. Burbacher TM, Ponce R, Grant KS (2015) Chap. 6 - The role of methylmercury exposure in neurodevelopmental and neurodegenerative disorders. In: Aschner, M. (Ed.). https://doi.org/10.1016/B978-0-12-800228-5.00006-6
4. China soil pollution investigation Bulletin, 2014, Ministry of Ecology and Environment of the Peopole's Republic of China. Ministry of Natural Resources of the People's Republic of China.
5. Chen MQ, Lu GN, Wu JX, Sun JT, Yang CF, Xie YY, Wang KF, Deng FC, Yi XY, Dang Z (2020) Acidity and metallic elements release from AMD-affected river sediments: Effect of AMD standstill and dilution. Environmental Research 186:109490. https://doi.org/10.1016/j.envres.2020.109490
6. Chen J, Chen Y, Liu LW, Ji JF, Balsam W, Sun YB, Lu HY (2006) Zr/Rb ratio in the Chinese loess sequences and its implication for changes in the East Asian winter monsoon strength. Geochimica et Cosmochimica Acta 70: 1471–1482. https://doi.org/10.1016/j.gca.2005.11.029
7. Chen ZQ, Ai YW, Fang C, Wang KX, Li W, Liu S, Li CL, Xiao JY, Huang ZY (2014) Distribution and phytoavailability of heavy metal chemical fractions in artificial soil on rock cut slopes alongside railways. Journal of Hazardous Materials 273: 165–173. https://doi.org/10.1016/j.jhazmat.2014.03.042
8. Cruz ACF, Gussochoueri PK, De Araujo, GS, Campos BG, Abessa DMS (2019) Levels of metals and toxicity in sediments from a Ramsar site influenced by former mining activities. Ecotoxicology and Environmental Safety 171: 162–172. https://doi.org/10.1016/j.ecoenv.2018.12.088
9. Cullen JT, Maldonado MT (2013) Biogeochemistry of cadmium and its release to the environment. Metal Ions in Life Science 11: 31–62. https://doi.org/10.1007/978-94-007-5179-8_2
10. Dosseto A, Buss HL, Chabaux F (2014) Age and weathering rate of sediments in small catchments: the role of hillslope erosion. Geochimica et Cosmochimica Acta 132(3): 238–258. https://doi.org/10.1016/j.gca.2014.02.010
11. Feng WK, Huang RQ, Xu Q (2009) The enlightenment of microstructure characteristic and mechanical behavior of rock. Research of Soil and Water Conservation 16(6):4. (in Chinese) https://doi.org/1005-3409(2009)06-0026-04
12. Gobe G, Crane D (2010) Mitochondria, reactive oxygen species and cadmium toxicity in the kidney. Toxicology Letters 198(1): 49–55. https://doi.org/10.1016/j.toxlet.2010.04.013

13. Hamon RE, McLaughlin MJ, Gilkes RJ, Rate AW, Zarcinas B, Robertson A, Cozens G, Radford N, Bettenay L (2004) Geochemical indices allow estimation of heavy metal background concentrations in soils. Global Biogeochemical Cycles 18(1):GB1014. https://doi.org/10.1029/2003GB002063
14. Han JL, Liang LC, Zhu YR, Xu XH, Wang L, Shang LH, Wu P, Wu QX, Qian XL, Qiu GL, Feng XB (2022) Heavy metal(loid)s in farmland soils on the karst plateau, southwest china: an integrated analysis of geochemical baselines, source apportionment, and associated health risk. Land Degradation and Development 33(10):1689–1703. https://doi.org/10.1002/ldr.4257
15. Hawleyn N (2000) Sediment resuspension near the Keweenaw Peninsula Lake Superior during the fall and winter 1990–1991. Journal of Great Lakes Research 26(4):495–505. https://doi.org/10.1016/S0380-1330(00)70711-8
16. Inoue T, Yamaguchi S, Nelson JM (2017) The effect of wet-dry weathering on the rate of bedrock river channel erosion by saltating gravel. Geomorphology 285:152–161. https://doi.org/10.1016/j.geomorph.2017.02.018
17. Islam MS, Hossain MB, Matin A, Sarker SI (2018) Assessment of heavy metal pollution, distribution and source apportionment in the sediment from feni river estuary, Bangladesh. Chemosphere 202:25–32. https://doi.org/10.1016/j.chemosphere.2018.03.077
18. Jarup L, Berglund M, Elinder CG, Nordberg G, Vahter M (1998) Health effects of cadmium exposure a review of the literature and risk estimate. Scand. J. Work. Environ. Health 24 (Suppl. 1): 1–51
19. Jönsson J, Persson P, Sjöberg S, Lövgren L (2005) Schwertmannite precipitated from acid mine drainage: phase transformation, sulfate release and surface properties. Applied Geochemistry 20(1): 179–191. https://doi.org/10.1016/j.apgeochem.2004.04.008
20. Kasuya M (2000) Recent epidemiological studies on itai-itai disease as a chroniccadmium poisoning in Japan. Water Sci. Technol 42: 147–154. https://doi.org/10.2166/wst.2000.0563
21. Kelderman P, Ang'Weya RO, Rozari PD, Vijverberg T (2012) Sediment characteristics and wind-induced sediment dynamics in shallow Lake Markermeer, the Netherlands. Aquatic Sciences 74(2):1–13. https://doi.org/10.1007/s00027-011-0222-7
22. Kleven O, Laskemoen T, Lifjeld JT (2009) Sperm length in sand martins riparia riparia: a comment on helfenstein et al. Journal of Avian Biology 40:241–242. https://doi.org/10.1111/j.1600-048X.2009.04766.x
23. Landeghem KV, Baas JH, Mitchell NC, Wilcockson D, Wheeler AJ (2012) Reversed sediment wave migration in the Irish Sea, NW Europe: A reappraisal of the validity of geometry-based predictive modelling and assumptions. Marine Geology 295–298, 95–112. https://doi.org/10.1016/j.margeo.2011.12.004
24. Lasaga AC, Soler JM, Ganor J, Burch TE, Nagy KL (1994) Chemical weathering rate laws and global geochemical cycles. Geochimica et Cosmochimica Acta 58(10): 2361–2386. https://doi.org/10.1016/0016-7037(94)90016-7
25. Lavergren U, AStrom ME, Falk H, Bergback B (2009) Metal dispersion in groundwater in an area with natural and processed black shale – nationwide perspective and comparison with acid sulfate soils. Applied Geochemistry 24(3), 359–369. https://doi.org/10.1016/j.apgeochem.2008.11.022
26. Li BY, Wei DN, Zhou YM., Huang YY, Tie BQ, Lei M (2021) Mechanisms of arsenate and cadmium co-immobilized on ferrihydrite inferred from ternary surface configuration. Chemical Engineering Journal 424:130410. https://doi.org/10.1016/j.cej.2021.130410
27. Li S, Ni SB (1997) The chemical abundance of the China mainland lithosphere. Geology and Prospecting 33(1): 31–38. (In Chinese) https://doi.org/CNKI:SUN:DZKT.0.1997-01-011
28. Liang L, Sun Y, Beets CJ, Prins MA, Feng W, Vandenberghe J (2013) Impacts of grain size sorting and chemical weathering on the geochemistry of jingyuan loess in the northwestern chinese loess plateau. Journal of Asian Earth Sciences 69:177–184. https://doi.org/10.1016/j.jseaes.2012.12.015
29. Liu HM, Zhang S, Song GQ, Zhang SP, Hao XF, Xie ZH, Xu NN, Liu P (2017) A Discussion on the Origin of Shale Reservoir Inter-Laminar Fractures in the Shahejie Formation of Paleogene, Dongying Depression. Journal of Earth Science 28(6): 1064–1077. https://doi.org/10.1007/s12583-016-0946-3
30. Liu HQ, Zhang Y, Yuan ZJ, Sun C (2021) Risk assessment concerning the heavy metals in sediment around Taihu Lake, China. Water Environment Research 93(11):2795–2806. https://doi.org/10.1002/wer.1638
31. Liu J, Zhu RL, Ma LY, Fu HY, Lin XJ, Parker SC, Molinari M (2021) Adsorption of phosphate and cadmium on iron (oxyhydr)oxides: A comparative study on ferrihydrite, goethite, and hematite. Geoderma 383(1):114799. https://doi.org/10.1016/j.geoderma.2020.114799
32. Liu YZ, Xiao TF, Zhu ZJ, Ma L, Li H, Ning ZP (2020) Geogenic pollution, fractionation and potential risks of cd and zn in soils from a mountainous region underlain by black shale. Science of The Total Environment 760(1): 143426. https://doi.org/10.1016/j.scitotenv.2020.143426
33. Liu YZ, Xiao TF, Perkins RB, Zhu JM, Zhu ZJ, Xiong Y, Ning ZP (2017) Geogenic cadmium pollution and potential health risks, with emphasis on black shale. Journal of Geochemical Exploration 176:42–49. https://doi.org/10.1016/j.gexplo.2016.04.004
34. Ma X. M., Lu N., Zhou K., et al. Quantitative determination of zinc, Aluminium, Cadmium and Silver in high-purity tin by ICP-MS. China Measurement & Test, 2018,44(6):38–41 (in Chinese) https://doi.org/10.11857/j.issn.1674-5124.2018.06.008

35. Maddela NR, Kakarla D, García LC, Chakraborty S, Venkateswarlu K, Megharaj M (2020) Cocoa-laden cadmium threatens human health and cacao economy: a critical view. Science of The Total Environment 720: 137645. https://doi.org/10.1016/j.scitotenv.2020.137645
36. Miller CJ, Rose AL, Waite TD (2009) Impact of natural organic matter on h2o2-mediated oxidation of Fe(II) in a simulated freshwater system. Geochimica Et Cosmochimica Acta 73(10): 2758–2768. https://doi.org/10.1016/j.gca.2009.02.027
37. Mndrescu M, Haliuc A, Zhang WG, Carozza L, Carzza JM, Groparu T, Valette P, Sun QL, Nian XM, Gradinaru I (2022) A 600 years sediment record of heavy metal pollution history in the danube delta. Science of The Total Environment 823:153702. https://doi.org/10.1016/j.scitotenv.2022.153702
38. Philipp L, Kai N, Sergiy A (2019) Classification of Fine Particles Using the Hydrodynamic Forces in the Boundary Layer of a Membrane. Chemie-Ingenieur-Technik 91(11):1656–1662. https://doi.org/10.1002/cite.201900052
39. Qin J, Huh Y, Edmond JM, Du G, Ran J (2006) Chemical and physical weathering in the min jiang, a headwater tributary of the yangtze river. Chemical Geology 227(1–2): 53–69. https://doi.org/10.1016/j.chemgeo.2005.09.011
40. Riebe CS, Kirchner JW, Finkel RC (2003) Long-term rates of chemical weathering and physical erosion from cosmogenic nuclides and geochemical mass balance. Geochimica Et Cosmochimica Acta 67(22): 4411–4427. https://doi.org/10.1016/S0016-7037(03)00382-X
41. Rola LD, Zanetti E, Duarte J (2013) Evaluation of semen characteristics of the species mazama americana in captivity. Animal Production Science 53(5): 472–477. https://doi.org/10.1071/AN12247
42. Rusk B, Reed M (2002) Scanning Electron Microscope-Cathodoluminescence Analysis of Quartz Reveals Complex Growth Histories in Veins from the Butte Porphyry Copper Deposit, Montana. Geology 30(8): 727–730. https://doi.org/10.1130/0091-7613(2002)030<0727:SEMCAO>2.0.CO;2
43. Song MY (2009) Supergenic geochemistry and environmental effects of selenium and heavy metals in the lower Cambrian black series of western Zhejiang Provenic, China. Hefei University of Technology. (in Chinese)
44. Tan LL, Ong WJ, Chai SP, Goh BT, Mohamed AR (2015) Visible-Light-Active Oxygen-Rich TiO_2 Decorated 2D Graphene Oxide with Enhanced Photocatalytic Activity Toward Carbon Dioxide Reduction. Applied Catalysis B: Environmental 179: 160–170. https://doi.org/10.1016/j.apcatb.2015.05.024
45. Tarun K, Dalai S, Krishnaswami M, Sarin MM (2012) Barium in the yamuna river system in the himalaya: sources, fluxes, and its behavior during weathering and transport. Geochemistry Geophysics Geosystems 3(12):1–23. https://doi.org/10.1029/2002GC000381
46. Wang DJ, Su CM, Zhang W, Hao XZ, Cang L, Wang YJ Zhou DM (2014) Laboratory assessment of the mobility of water-dispersed engineered nanoparticles in a red soil (ultisol). Journal of Hydrology 519:1677–1687. https://doi.org/10.1016/j.jhydrol.2014.09.053
47. Waychunas GA, Kim CS, Banfield JF (2005) Nanoparticulate iron oxide minerals in soils and sediments: unique properties and contaminant scanvenging mechanisms. Journal of Nanoparticle Research 7(4):409–433. https://doi.org/10.1007/s11051-005-6931-x
48. Williams JA, Antoine J (2020) Evaluation of the elemental pollution status of jamaican surface sediments using enrichment factor, geoaccumulation index, ecological risk and potential ecological risk index. Marine Pollution Bulletin 157: 111288. https://doi.org/10.1016/j.marpolbul.2020.111288
49. Xin RH, Sui XX (2022) Geochemical characteristics of the heavy metals in soil,the south of Xuancheng, Anhui Province. Acta Petrologica et Mineralogica 41(1):185–194. (in Chinese) https://doi.org/1000-6524(2022)01-0185-10
50. Yang Q, Yang Z, Filippelli GM, Ji JF, Ji WB, Liu X, Wang L, Yu T, Wu TS, Zhuo XX, Zhang QZ (2021) Distribution and secondary enrichment of heavy metal elements in karstic soils with high geochemical background in guangxi, china. Chemical Geology 567: 120081. https://doi.org/10.1016/j.chemgeo.2021.120081
51. Yang WJ, Ding KB, Zhang P, Qiu H, Cloquet C, Wen HJ, Morel JJ, Qiu RL, Tang YT (2018) Cadmium stable isotope variation in a mountain area impacted by acid mine drainage. The Science of the total environment 646:696–703. https://doi.org/10.1016/j.scitotenv.2018.07.210
52. Zhang W, Long JH, Zhang XR, Shen WN, Wei ZY (2020) Pollution and ecological risk evaluation of heavy metals in the soil and sediment around the htm tailings pond, northeastern China. International Journal of Environmental Research and Public Health 17(19): 7072. https://doi.org/10.3390/ijerph17197072
53. Zhao WF, Song GX, Guan DX., Ma Q, Guo C, Wen YB, Ji JF (2018) Pollution status and bioavailability of heavy metals in soils of a typical black shale area. Journal of Agro-Environment Science 37(7): 1332–1341. (in Chinese) https://doi.org/10.11654/jaes.2018-0595
54. Zhou WD, Xiang W, Jin L, Li CH, Zheng W (2020) The Self-Purification Mechanism and Control Countermeasures of Cadmium-Rich Acid Mine Drainage of Stone Coal Mines. Environmental Science & Technology 43(8):20–27. (in Chinese) https://doi.org/10.19672/j.cnki.1003-6504.2020.08.004
55. Zhu K, Hopwood MJ, Groenenberg JE, Engel A, Achterberg EP, Gledhill M (2021) Influence of ph and dissolved organic matter on iron speciation and apparent iron solubility in the peruvian shelf and slope region. Environmental Science and Technology 55(13): 9372–9383. https://doi.org/10.1021/acs.est.1c02477

Figures

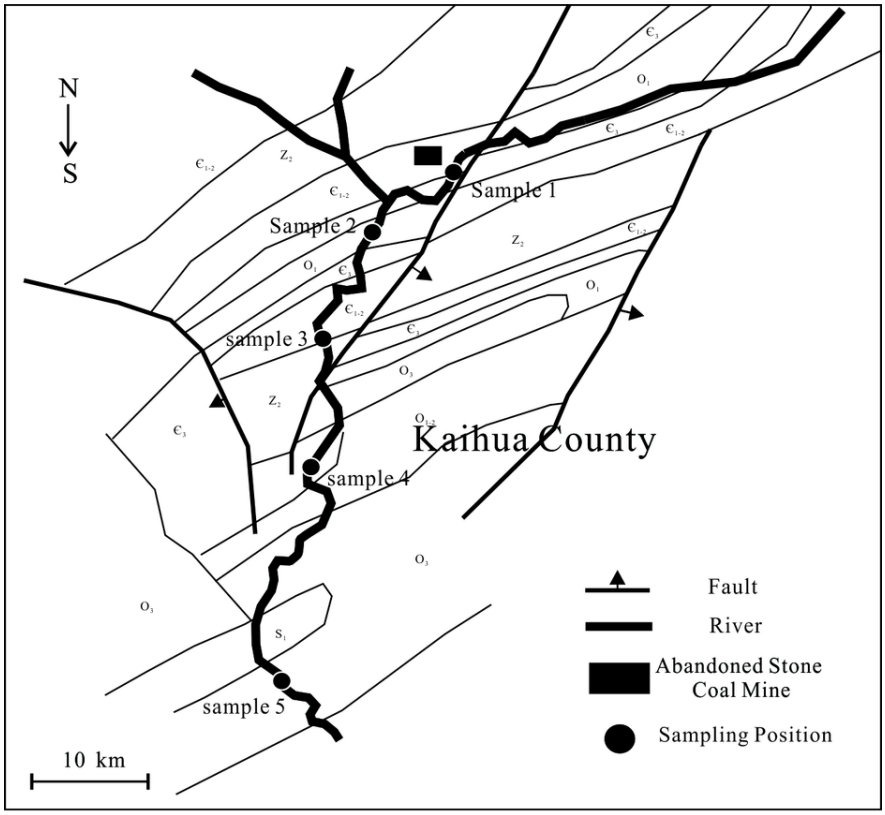

Figure 1

The distribution of rock units in the region traversed by the river within the study area (water flows from north to south)

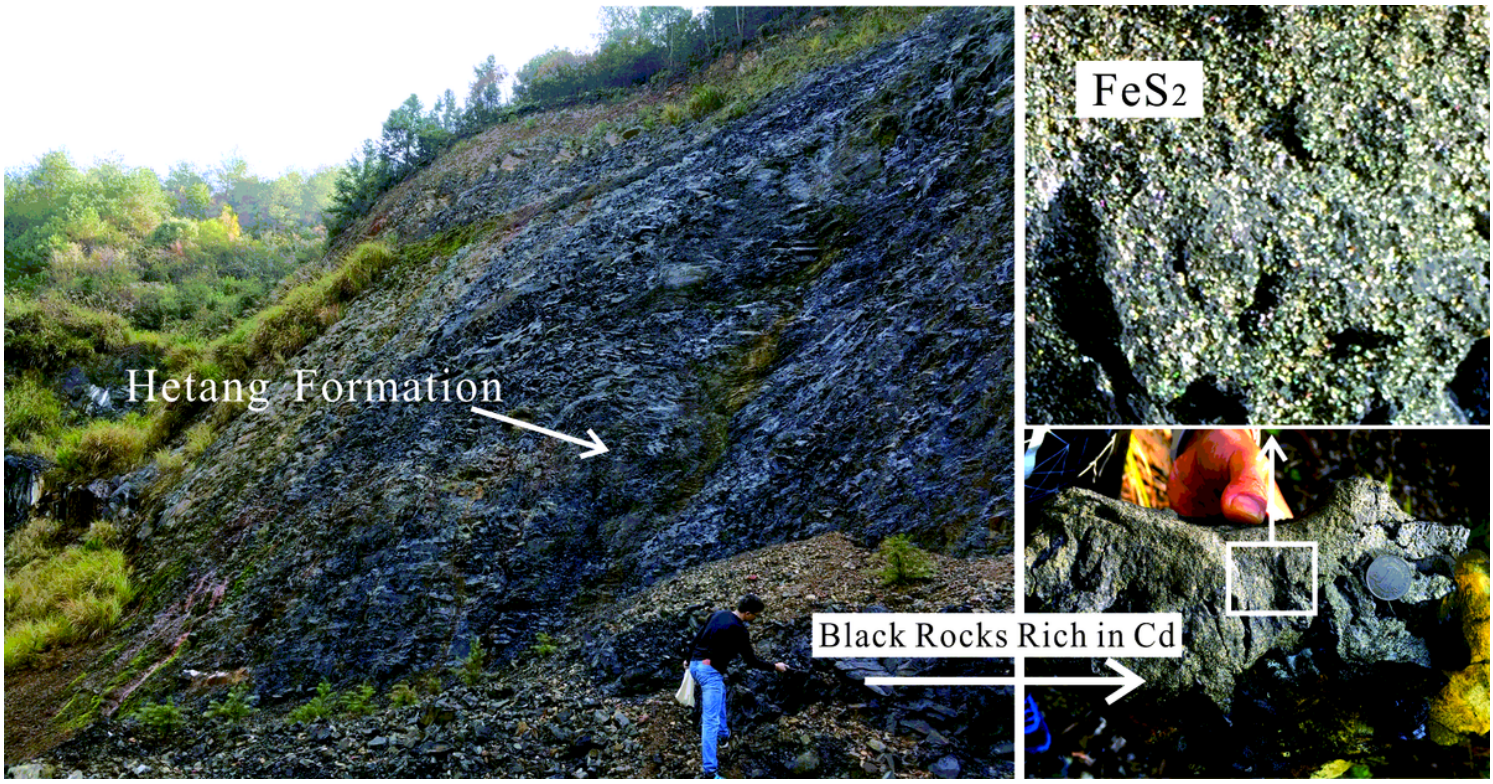

Figure 2

Black shales of the Hetang Formation exhibit a high concentration of cadmium

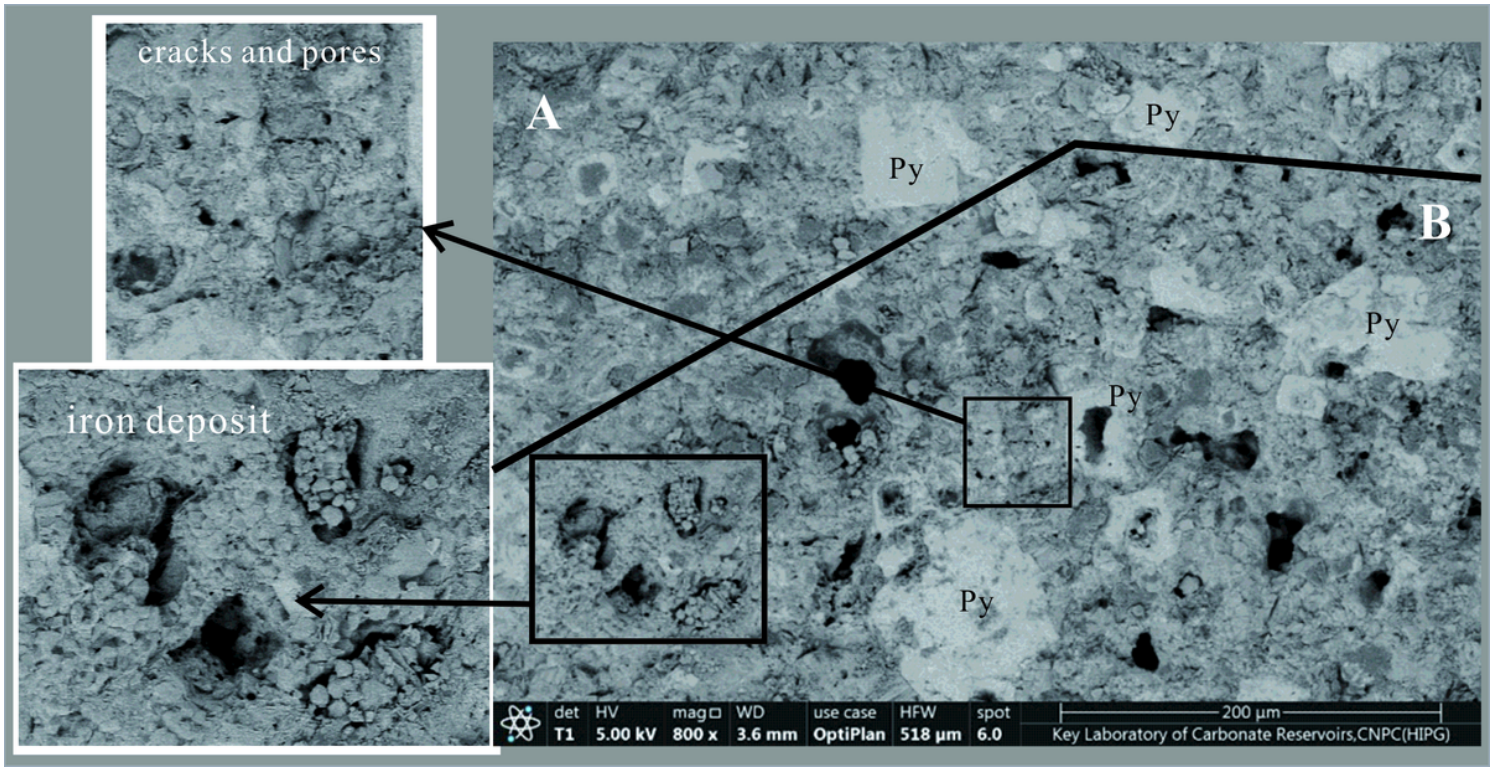

Figure 3

Rock fragments from the Hetang formation in sample 1. Area A: unweathered area with no obvious pores and cracks, pyrite is basically not corroded; Area B: weathered area with more pores and cracks due to weathering, pyrite is largely corroded and granular iron deposits appear.

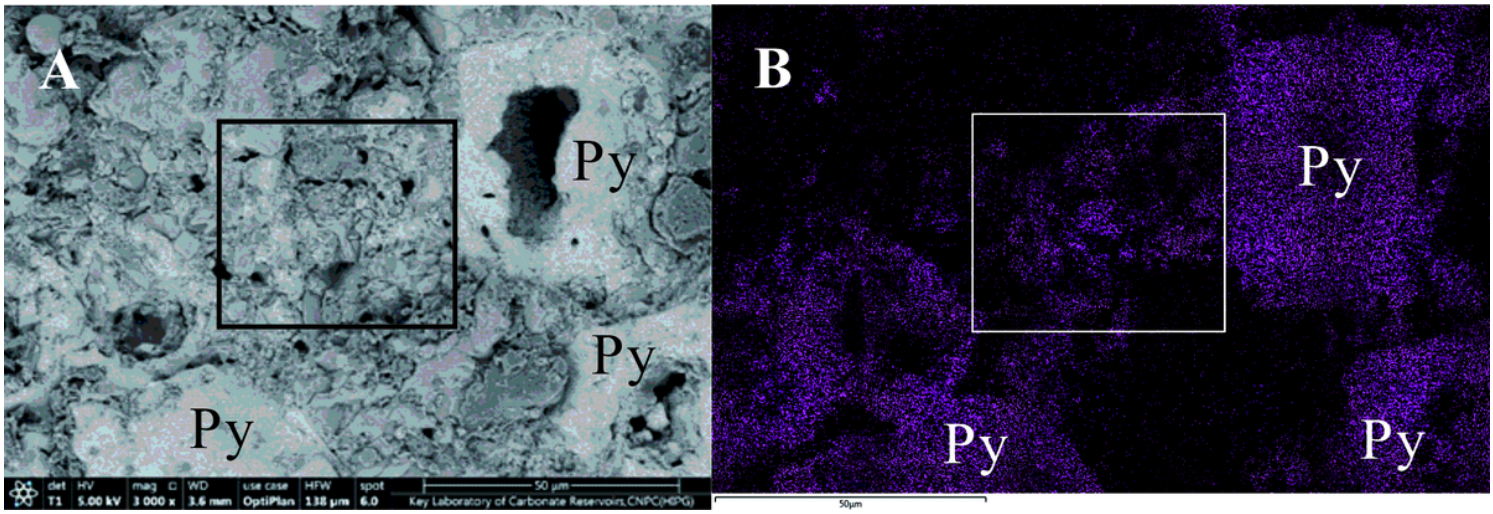

Figure 4

In the rock debris of the Hetang formation, due to the dissolution of pyrite, small iron deposits are filled between the pores (within the white frame). A. Mineral composition under scanning electron microscope; B. Iron element distribution status, pink dots are iron element accumulation areas.

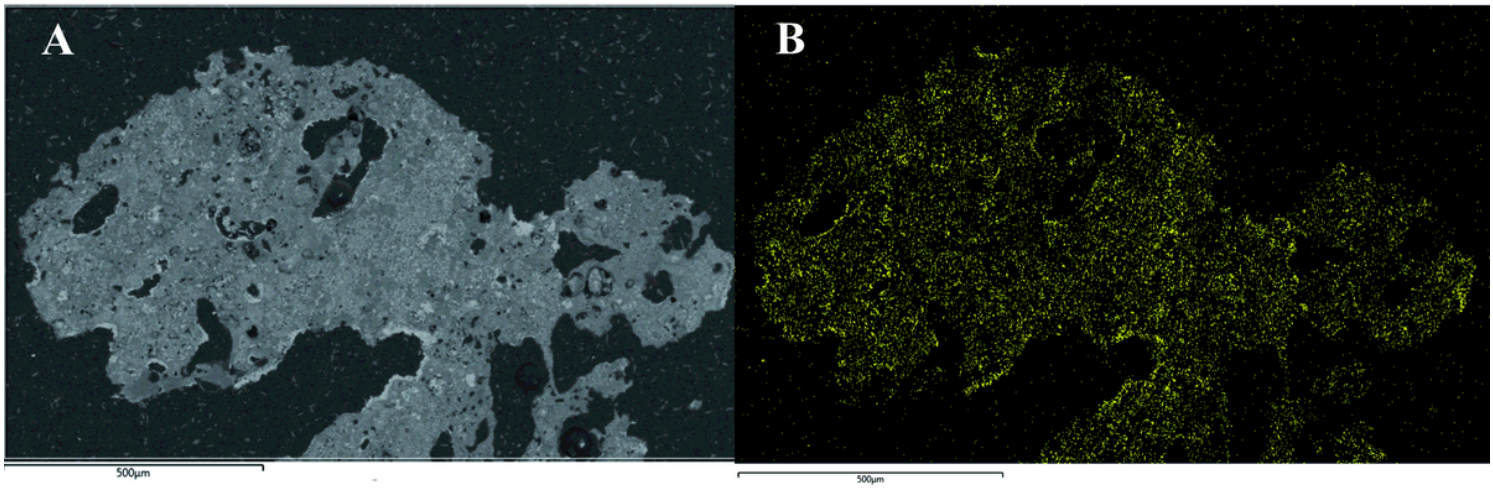

Figure 5

Severely weathered rock debris of the Hetang formation, with a large amount of damaged pyrite mold cavities remaining. A. Rock debris morphology under scanning electron microscope; B. The iron element distribution in rock fragments is uniform.

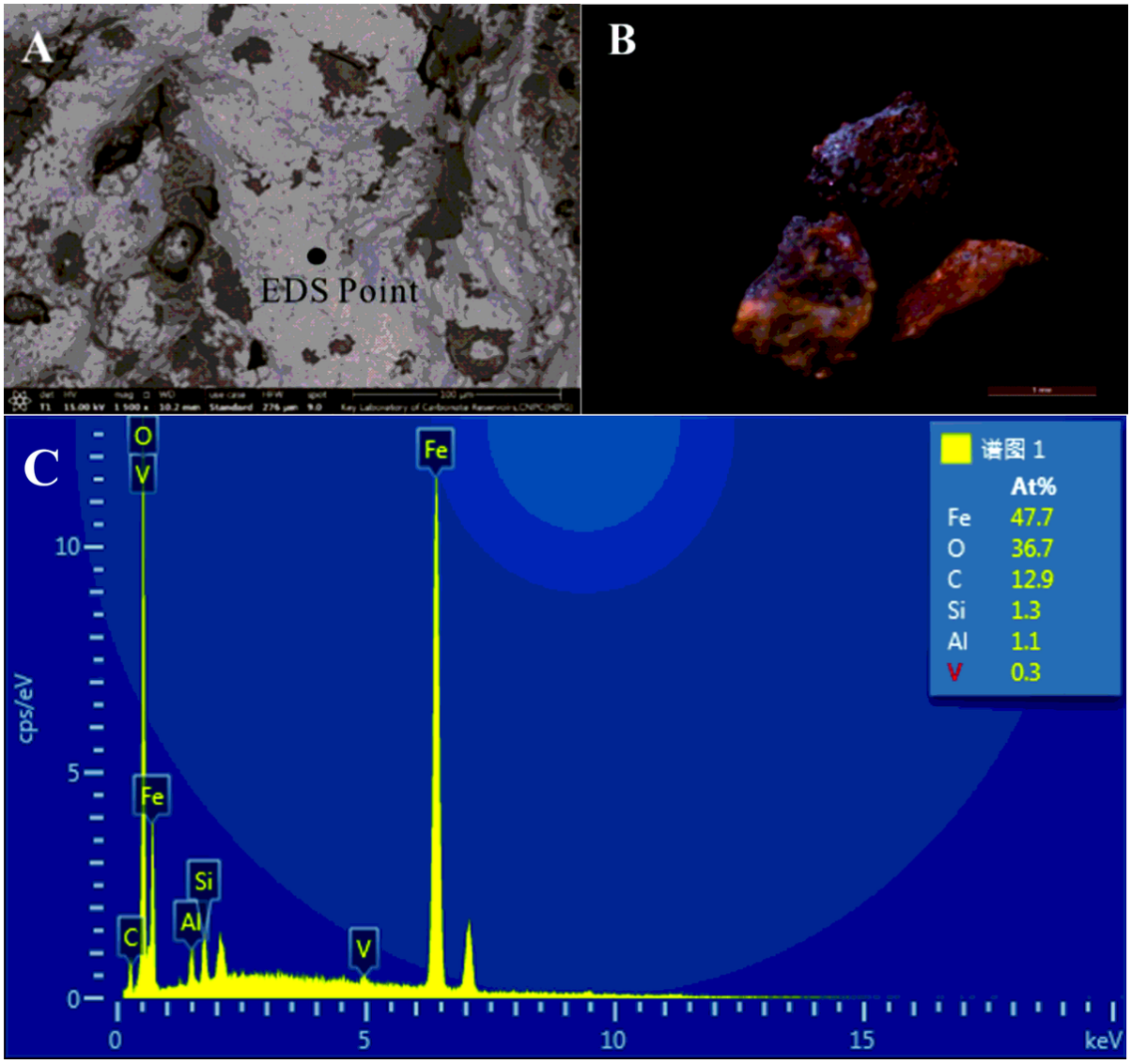

Figure 6

Weathered rock debris from Hetang formation in Sample 2. A. Lacquer -like iron-sediment on the surface of rock debris; B. The surface of rockdebris is covered with a large amount of stable iron-sediment such as limonite, which are yellowish-brown in color. C. EDS results of lacquer -like iron-sediment.

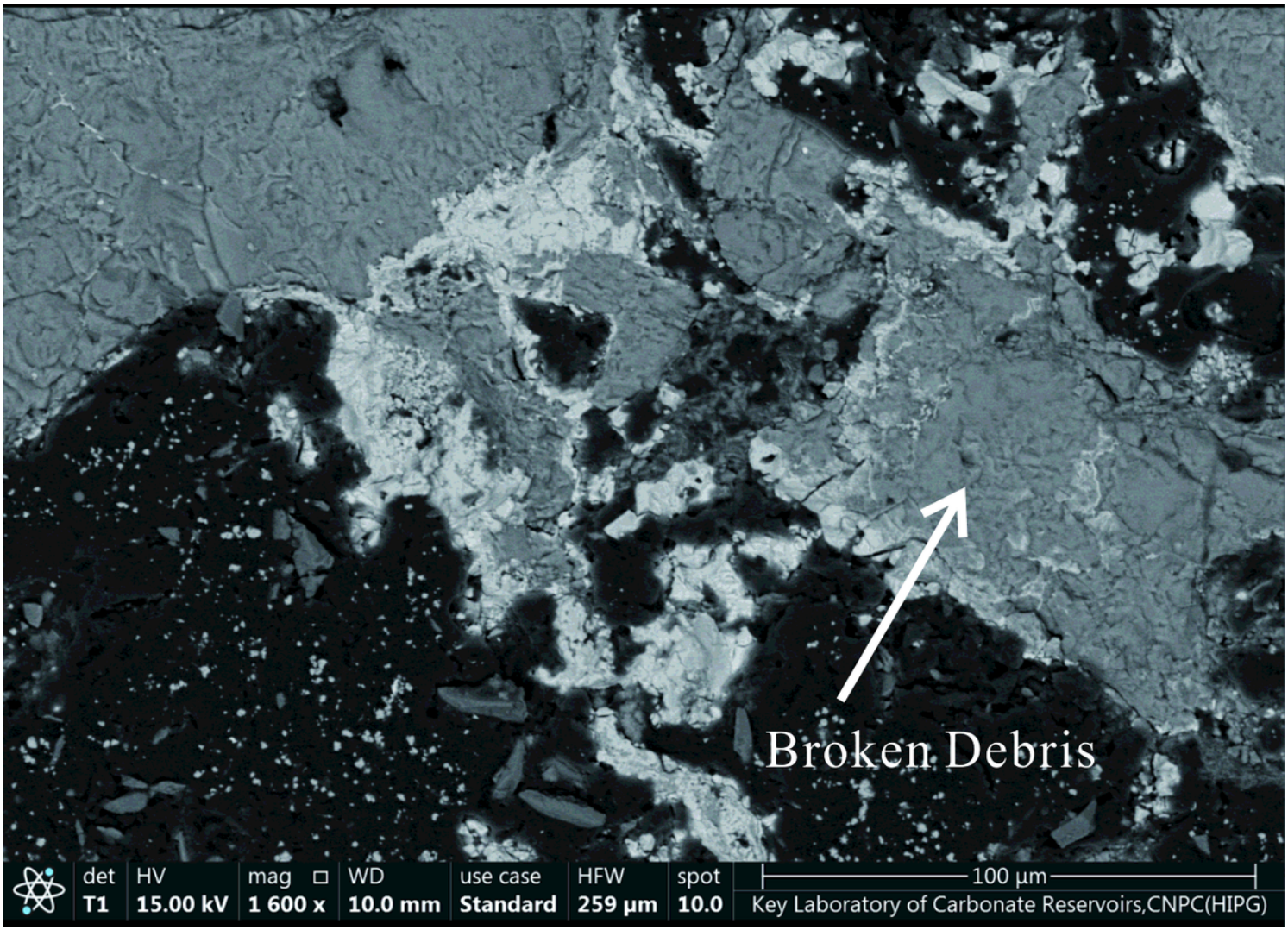

Figure 7

Broken lotus pond rock debris in sample 2. The brighter low-gray part is cadmium-containing iron-sediment.

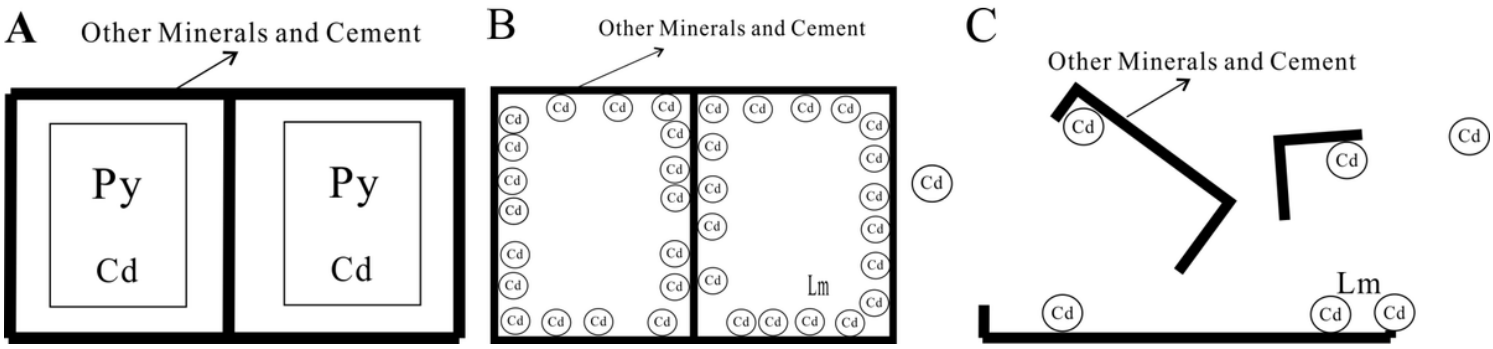

Figure 8

Cadmium-containing Hetang formation rock debris gradually disintegrates during weathering, and the schematic diagram of the change in cadmium occurrence state. A. The rock debris structure is stable, pyrite is not obviously weathered, and cadmium exists in pyrite; B. The rock debris structure is partially destroyed, pyrite is partially weathered and eroded, cadmium begins to enter the water environment and partly exists in residual pyrite and ferrihydrite and limonite; C. The rock debris is completely weathered, difficult to weather mineral residues are broken, a large amount of cadmium loss enters the water environment, a small part remains on the surface of ferrihydrite and limonite in the rock debris.

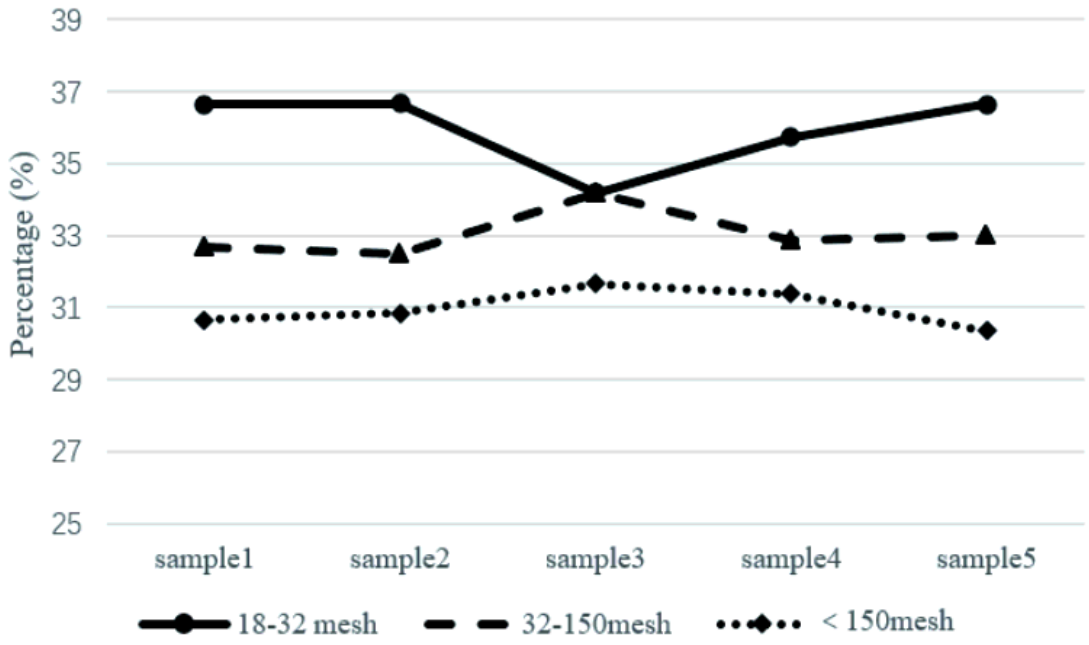

Figure 9

Rock debris content of different grain levels in the sample (mass ratio)

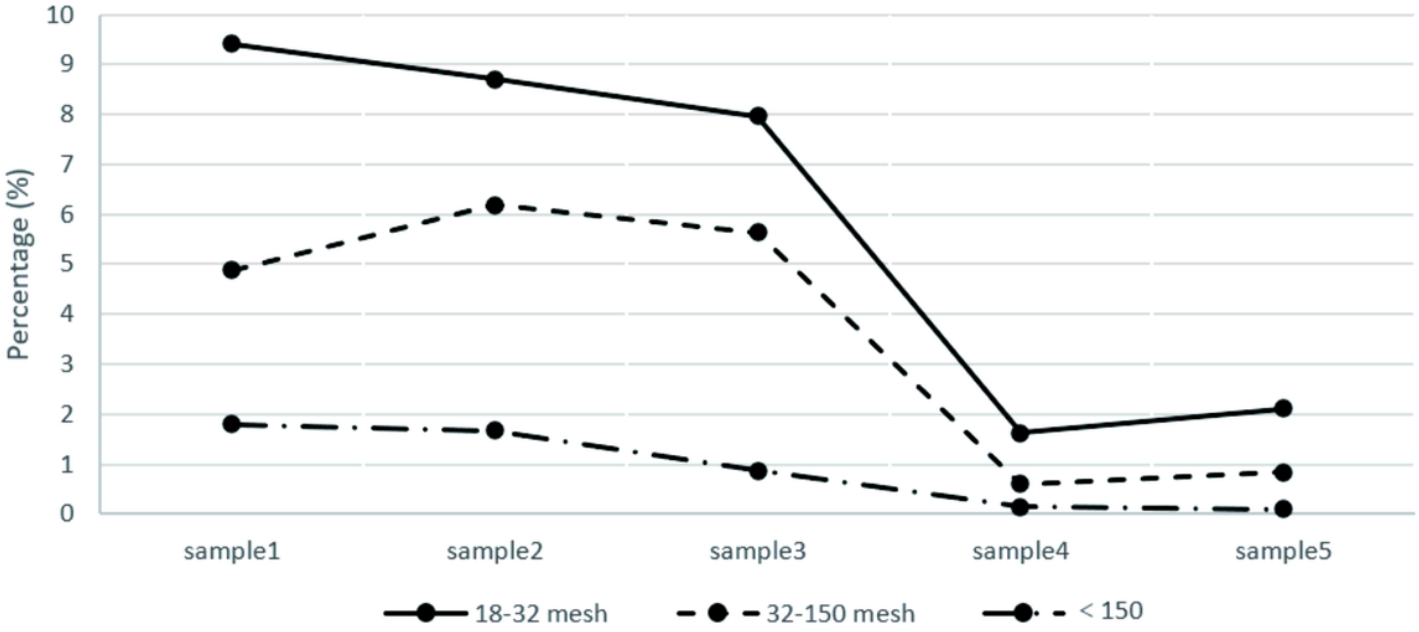

Figure 10

The content of rock debris in the Hetang formation in each grain grade of the sample